Effects of Sustained Antiangiogenic Therapy in Multistage Prostate Cancer in TRAMP Model

Tatyana Isayeva, Diptiman Chanda, Lisa Kallman, Isam-Eldin A. Eltoum, and Selvarangan Ponnazhagan

Department of Pathology, The University of Alabama at Birmingham, Birmingham, Alabama

Abstract

Antiangiogenic therapy is a promising alternative for prostate cancer growth and metastasis and holds great promise as an adjuvant therapy. The present study evaluated the potential of stable expression of angiostatin and endostatin before the onset of neoplasia and during the early and late stages of prostate cancer progression in transgenic adenocarcinoma of mouse prostate (TRAMP) mice. Groups of 5-, 10-, and 18-week-old male TRAMP mice received recombinant adeno-associated virus-6 encoding mouse endostatin plus angiostatin (E+A) by i.m. injection. The effects of therapy were determined by sacrificing groups of treated mice at defined stages of tumor progression and following cohorts of similarly treated mice for long-term survival. Results indicated remarkable survival after recombinant adeno-associated virus–(E+A) therapy only when the treatment was given at an earlier time, before the onset of high-grade neoplasia, compared with treatment given for invasive cancer. Interestingly, early-stage antiangiogenic therapy arrested the progression of moderately differentiated carcinoma to poorly differentiated state and distant metastasis. Immunohistochemical analysis of the prostate from treated mice indicated significantly lower endothelial cell proliferation and increased tumor cell apoptosis. Vascular endothelial growth factor receptor (VEGFR)-2 expression was significantly down-regulated in tumor endothelium after treatment but not VEGFR-1. Analysis of the neuroendocrine marker synaptophysin expression indicated that antiangiogenic therapy given at an early-stage disease reduced neuroendocrine transition of the epithelial tumors. These studies indicate that stable endostatin and angiostatin gene therapy may be more effective for minimally invasive tumors rather than advanced-stage disease. [Cancer Res 2007;67(12):5789–97]

Introduction

Prostate cancer is one of the leading causes of cancer death in men (1). Current treatment for localized prostate cancer includes radical prostatectomy, cryoablation therapy, external beam radiation therapy, and brachytherapy (2–4). Androgen ablation therapy and chemotherapy are given for patients with locally advanced and metastatic disease (2). Despite recent advances in early detection, occurrence of metastatic disease due to androgen independence and resistance to conventional therapies is common. Thus, evaluation of newer therapies that can limit local advancement of primary tumors necessary to develop distant metastasis would be effective treatments of prostate cancer.

Antiangiogenic therapy is highly promising as an adjuvant therapy to overcome some of the limitations of conventional therapies for antitumor effects. Clinical trials with compounds having antiangiogenic effects, including carboxyamido-triazole, thalidomide, TNP-470, and interleukin-12, have shown promise (5). Most of these studies were done in patients with advanced-stage disease with well-established tumor vasculature and activation of several angiogenic and growth factor signals (6). Thus, it is important to determine the potential of antiangiogenic therapy at progressive stages of prostate cancer growth to identify the most effective stage for treatment and to delineate mechanistic implications. The present study describes the effects of sustained endostatin and angiostatin therapy at different grades of tumor pathology in the transgenic adenocarcinoma of mouse prostate (TRAMP) model. TRAMP mice develop progressive forms of prostate cancer during their lifetime with lesions ranging from mild prostatic intraepithelial neoplasia (PIN) to large multinodular malignant neoplasia (7). Histopathology of the prostate and molecular changes associated with the progression of the disease have been well characterized in the TRAMP model, which allows a careful examination of the effects of new interventional therapies. Influenced by the transactivation of probasin promoter expressing the SV40 large-T antigen during puberty, tumorigenesis occurs in 100% these, and different stages of the cancer proceed as in humans (7).

Because antiangiogenic therapy mandates sustained amounts of the angiosuppressive factor(s) for therapeutic effect, we chose a gene transfer approach to deliver them from a recombinant adeno-associated virus (rAAV). Our earlier studies established that stable expression of angiostatin and endostatin as secreted proteins from rAAV-transduced muscle tissue provides significant protection against the growth of human cancer cell lines as xenografts in athymic mice (8, 9). We have also recently established that transduction of rAAV, encapsidated in serotype 6 capsid, provides significant enhancement of transgene expression over rAAV2 (10). Thus, in the present study, we used rAAV6 vector to produce systemically stable levels of angiostatin and endostatin beginning at the preneoplastic lesion, hyperplasia, or adenocarcinoma stages of prostate cancer growth in TRAMP model.

Results of these studies indicated that stable expression of angiostatin and endostatin in early-stage disease not only delayed progression of the disease but also significantly increased survival. Histopathology of prostate tissue from mice with long-term survival revealed arrest of cancer progression. This blockade greatly inhibited organ metastasis. Sustained expression of angiostatin and endostatin significantly reduced vascular endothelial growth factor (VEGF) receptor (VEGFR)-2 expression as well as

Requests for reprints: Selvarangan Ponnazhagan, Department of Pathology, The University of Alabama at Birmingham, LHRB 513, 701, 19th Street South, Birmingham, AL 35294-0007. Phone: 205-934-6731; Fax: 205-975-9927; E-mail: sponnazh@path.uab.edu.

doi:10.1158/0008-5472.CAN-06-3637

neuroendocrine transition of the prostate epithelium. However, the same therapy was ineffective in increasing overall survival when given after formation of an established tumor. These data indicate that stable antiangiogenic therapy may greatly improve the outcome of prostate cancer when administered during an early stage of the disease rather than during a late stage of the disease, and may be effectively combined with conventional therapies for a synergistic benefit.

Materials and Methods

Cells and reagents. Human embryonic kidney cell line 293 was purchased from the American Type Culture Collection and maintained in Iscove's modified essential medium supplemented with 10% newborn calf serum. The cells were cultured at 37°C with 5% CO_2. Restriction endonucleases and other modifying enzymes were purchased from either New England Biolabs or Promega Co. TRAMP-C2 and TRAMP-C3 cells were a kind gift of Dr. Norman Greenberg and maintained as described (11). Primary human umbilical vein endothelial cells were maintained as published (8). Mouse monoclonal antibody for Ki67 (clone SP6) and rabbit polyclonal antibody for poly(ADP-ribose) polymerase (PARP) p85 fragment were obtained from Research Diagnostics, Inc., and Promega, respectively. Rat anti-mouse CD31 antibody (clone MEC 13.3) was purchased from BD PharMingen. Antibodies for mouse hypoxia inducible factor (Hif)-1α, VEGFR1, and VEGFR2 were purchased from R&D Systems, Inc. Antibody for mouse synaptophysin was purchased from Santa Cruz Biotechnology. A monoclonal rabbit anti-mouse cytokeratin-8 antibody (clone E432) was purchased from Abcam, Inc. Horseradish peroxidase (HRP)–conjugated and Alexa Fluor–conjugated secondary antibodies were purchased from Amersham and Molecular Probes, respectively. Color reagents were purchased from Amersham. The mouse VEGF ELISA kit was purchased from R&D, and mouse endostatin ELISA kit was from Neogen Corporation. Antibodies for angiostatin ELISA were purchased from Alpha Diagnostics Intl., Inc.

Transgenic mice. The TRAMP mice, developed on a pure C57BL/6 background, heterozygous for the probasin-Tag transgene, were bred and maintained in the Animal Care Facility of the University of Alabama at Birmingham. Transgenic males and the nontransgenic littermates were obtained as (TRAMP C57BL/6 × FVB Breeder) F_1. After weaning at 3 to 4 weeks of age, genotyping for the probasin-Tag transgene was done by PCR using DNA isolated from tail biopsy (12). Animal care and treatments were conducted in accordance with established guidelines and protocols approved by the University of Alabama at Birmingham Institutional Animal Care Committee.

Recombinant plasmids, production, and purification of rAAV. cDNA containing murine endostatin and angiostatin sequences were isolated from the plasmid pBlast murine Endo::Angio (Invivogen) and subcloned in the AAV plasmid pSub201 (13) between the inverted terminal repeats under the control of the cytomegalovirus enhancer/chicken β-actin promoter. Secretory signal sequences of mouse interleukin 2 and mouse plasminogen were included upstream of the endostatin and angiostatin cDNA, respectively, for systemic secretion. Construction of recombinant plasmids containing green fluorescent protein (GFP) was recently published (8). Production of rAAV was done by transient transfection in 293 cells using the helper plasmid containing adenovirus and AAV (Rep2-Cap6) functions (14). Recombinant virus was purified from cell lysates by iodixanol gradient centrifugation and heparin affinity column chromatography (15). The particle titer of purified virions was determined by quantitative slot blot analysis.

Vector injection, preparation, and analysis of tissues. Before initiating treatment studies, 25 male TRAMP mice and 10 age-matched male nontransgenic littermates were sacrificed at 12, 18, 24, 28, and 32 weeks of age to determine the pathology of the prostate, tumor grade, and index of metastasis. The accuracy of tumor grade at these time points was determined to be >80%. For treatment studies, 22 mice were included for sacrifice at each time point (12, 18, 24, 28, and 32 weeks; 110 mice in total) for pathologic evaluation, and 14 mice were included for end point survival. There were three time points for treatment with rAAV-GFP and rAAV-(E+A) namely 5, 10, and 18 weeks of age. Vector injections were given only once with 1×10^{11} genomic particles of rAAV-(E+A) or GFP i.m. in the quadriceps of the hind limb at 5, 10, or 18 weeks of age.

Mouse genitourinary tract, consisting of the bladder, urethra, seminal vesicles, ampullary gland, and prostate were excised and weighed. At necropsy, all animals were examined for gross organ abnormalities. The tissues were formalin-fixed and embedded in paraffin. Five-micrometer sections were stained with H&E. For the analysis of prostate, based on anatomic location and histologic features as described (12, 16), all prostate lobes, including anterior, ventral, and dorsolateral lobes, were reviewed by an experienced pathologist (Dr. Eltoum) in a blinded fashion and graded. Prostate lesions were scored using a 1 to 6 scale that has been established for TRAMP mice (16). Grade 1, normal prostate epithelium; grade 2, low PIN; grade 3, high PIN; grade 4, well-differentiated tumor; grade 5, moderately differentiated tumor; and grade 6, poorly differentiated tumor. The extent of PIN was quantified by recording the number of separate foci of PIN per section. Characteristics of PIN lesions were epithelial tufting, hyperchromatic nuclei, elongated nuclei, nuclear stratification, microcapillary projections, cribiform structures, and increased mitosis and apoptosis. Progression of PIN lesions to a higher grade was characterized by increased invasiveness of the tumor cells. Well-differentiated tumor was characterized by increased quantity of small glands, often associated with desmoplastic response or stromal thickening. Cells in well-differentiated tumors often exhibited round nuclei with fewer hyperchromatic nuclei than in PIN lesions. Increased apoptosis and mitosis were also apparent. Moderately differentiated tumors were characterized by nearly anaplastic sheets of cells with remnants of glandular architecture. Poorly differentiated tumors were characterized by anaplastic sheets of cells with irregular nuclei and a decrease in the cytoplasmic region. This tumor grade is often highly vascularized and hemorrhagic, and the cancer lesions are also necrotic. End point in survival studies was based on death or when the animals became totally ill and moribund. At that time, mice were humanely euthanized by Institutional Animal Care and Use Committee–approved protocol and the date of euthanasia was recorded as the end day of survival. Following euthanasia, autopsy was done and end-stage (grade 6) tumor was confirmed by histopathology.

Blood vessel diameter was measured in 10 random fields per tissue sample of highest vascular density at ×20 magnification in an Olympus microscope. Tissues from a minimum of 10 mice were analyzed for each group. The images were analyzed using Bioquant Nova Software (Bioquant Image Analysis Corporation).

Immunohistochemistry. Immunohistochemical studies were done in 5-μm sections of paraffin-embedded tumor tissues using antibodies for Ki67, anti-PARP p85, CD31, Hif-1α, VEGFR-1, VEGFR-2, synaptophysin, and cytokeratin-8. For each group, tissues from at least 10 mice were analyzed. Antigen retrieval was achieved by incubating the slides in 0.05% trypsin for 20 min at 37°C and endogenous peroxidase was blocked by incubation with 3% H_2O_2 for 10 min at room temperature. The working dilutions of the antibodies were as follows: Ki67 and anti-PARP p85, 1:50; CD31/PECAM1, Hif-1α, VEGFR-1, and VEGFR-2, 1:10; cytokeratin-8, 1:200. Secondary antibodies were respective, isotype-matched, anti-rabbit, anti-rat, or anti-goat antibodies conjugated to HRP or Alexa Fluor, and were used at a dilution of 1:500. To determine the proliferation and apoptotic indices, stained slides were examined under high power (×40). A minimum of 10 randomly chosen fields were counted for slides from each mouse to determine the total number of cells and cells that stained positive in each field. The percentage proliferation and apoptosis was calculated using the following formula: (number of positively stained cells / total number of cells in a field) × 100. The antigen-antibody complex was visualized with diaminobenzidine tetrahydrochloride or fluorescent secondary antibody, and tissues were counterstained minimally with hematoxylin. To determine microvessel density, the number of vessels was determined by counting 10 fields of the highest vascular density in high-power (×40).

To determine whether tumor cells (cytokeratin-8 staining) or tumor-associated endothelial cells [CD31/platelet/endothelial cell adhesion

molecule 1 (PECAM-1) staining] expressed VEGR1, VEGFR2, and Hif-1α, we used a double-immunofluorescence staining technique. Cytokeratin-8– and CD31-positive cells were identified by red fluorescence (Alexa 594) and VEGR1- and VEGFR2-positive cells were identified by green fluorescence (Alexa 488). The presence of growth factor receptors on the cells were detected by colocalization of red and green fluorescence, which appeared yellow. The percentage of double-stained cells was determined from tumor cells or endothelial cell in 10 randomly selected microscopic fields at ×200 magnification (22 mice per group). Data from immunohistochemistry were further confirmed by quantitative real-time PCR described below.

ELISA. Blood samples from mice were allowed to clot for 2 h at room temperature at 4°C. The samples were centrifuged for 20 min at 2,000 × *g* and the serum was removed and stored at −80°C until assayed. For each time point, serum samples from at least 12 mice per group were analyzed. For ELISA, serum samples were diluted 10-fold. Endostatin and VEGF levels were measured as per instructions of the ELISA kit manufacturers. The sensitivity of the assays was 9.1 and 3 pg/mL for endostatin and VEGF, respectively. An ELISA was developed in our laboratory to determine serum angiostatin levels similar to that previously described (8). Briefly, 96-well ELISA plates were coated overnight at 4°C with a monoclonal angiostatin antibody (ANST12-M, Alpha Diagnostics Intl.) at a concentration of 10 μg/mL in borate buffer (BS; pH 8.6). The next day, the antibody was discarded and the wells were blocked with 150 μL of bovine serum albumin in BS (BS-BSA) for 45 min at room temperature. Serum samples, diluted 1:3 in BS-BSA, were added to the wells and incubated overnight at 4°C. All of the samples were analyzed in triplicate. After washing five times with PBS containing 0.5% Tween 20, a polyclonal angiostatin antibody (ANST11-S, Alpha Diagnostic Intl.), biotinylated using the EZ-Link Sulfo-NHS-LC-Biotin reagent (Pierce), was added at a concentration of 1 μg/mL and incubated overnight at 4°C. The contents were then discarded and plates were washed five times with PBS containing 0.5% Tween 20 after which streptavidin-conjugated alkaline phosphatase was added and incubated for 30 min at room temperature. Color development was done with the addition of pNPP chromogenic substrate (Sigma) and incubated at room temperature for 20 min. Absorbance at 405 nm was measured in an ELISA plate reader. As a reference standard, known concentrations of recombinant angiostatin from 0 to 1,000 ng/mL were included in triplicate. The sensitivity of the assay was 15 ng/mL.

Real-time PCR. Total RNA was isolated from the prostate tissue of naïve and rAAV-(E+A)–treated TRAMP mice (n = 22 mice per group) with TRIzol reagent (Invitrogen) and RNeasy Mini Kit (Qiagen). A two-step quantitative real-time, reverse transcription-PCR (RT-PCR) was done on cDNA generated with isolated RNA using the iScript cDNA Synthesis Kit and iQ SYBR Green Supermix (Bio-Rad). Primers used were as follows: mouse VEGFR1 forward, 5′-TCACCGAACTCCACCTCCATGTTT-3′ and reverse, 5-TATCTTCATG-GAGGCCTTGGGCTT-3; VEGFR2 forward, 5′-ACGTCGACATAGCCTC-CACTGTTT-3′ and reverse, 5′-TTCTCGGTGATGTACACGATGCCA-3′. Mouse *glyceraldehyde-3-phosphate dehydrogenase* (*GAPDH*) forward, 5′-TCAACAGCAACTCCCACTCTTCCA-3′ and reverse, 5′-ACCCTGTTGCT-GTAGCCGTATTCA-3′. Quantitative real-time PCR was carried out in a Bio-Rad *i*cycler (Optical Module). Reactions were done using the Light-Cycler-FastStart DNA Master SYBR Green system (Roche Molecular Biochemicals) in a final volume of 25 μL, consisting of 0.5 μL of each primer (0.5 pmol/L), 12.5 μL of 2× supermix containing reaction buffer, Fast-start Taq DNA double strand–specified SYBR Green I dye, 10.5 μL H_2O, and 1 μL (0.5 μg) of template DNA. PCR was done with a 3-min preincubation at 95°C followed by 45 cycles of 15-s denaturation at 95°C, and 1 min each for annealing and extension at 67°C. PCR products were subjected to melting curve analysis using the Light Cycler system to exclude amplification of nonspecific products. The values were normalized with GAPDH values from each sample.

Effects of endostatin and angiostatin in prostate cancer cells derived from the TRAMP mice. TRAMP-C2 and TRAMP-C3 cells, derived from TRAMP model (11), and human umbilical vascular endothelial cells (HUVEC) were mock-transfected or transfected with rAAV-(E+A) or rAAV-GFP in 96-well tissue culture plates. Seventy-two hours later, cell proliferation was determined by 3-(4,5-dimethylthiazol-2-yl)-2,5-diphenyltetrazolium bromide assay as described (8). Total RNA was isolated in similarly transfected cells and RT-PCR was done for the expression of VEGFR-1 and VEGFR-2. The values were normalized with RT-PCR data for GAPDH from same samples. All *in vitro* studies were done in triplicates.

Statistical analysis. Results were analyzed using a two-tailed Student's t test to assess statistical significance. Values of $P < 0.05$ were considered statistically significant.

Results

Disease progression in TRAMP mice. For an experimental model of prostate cancer, we independently bred and maintained a colony of TRAMP mice in C57BL/6 × FVB background at the University of Alabama at Birmingham animal facility. When these mice were 10 to 12 weeks old, they began to show PIN lesions in the prostate glands characterized by epithelial tufting, nuclear stratification, and micropapillary projection. The earliest adenocarcinoma was detected around 18 weeks. Tumor differentiation was characterized by increased mitoses and apoptosis. As the tumors became poorly differentiated, increased vascularization and hemorrhage was apparent and the tumor cells appeared pleomorphic with irregular nuclei. Prostate tumors continued to grow beyond age 28 weeks when some mice began to die of the illness. Major cause of death was due to organ metastasis of the prostate cancer, in particular to lung and lymph nodes. The mean age of survival of untreated mice was found to be 31.2 ± 5.6 weeks.

Systemically stable levels of antiangiogenic factors after rAAV transduction and its influences on VEGF. Cohorts of TRAMP mice were given a one-time i.m. injection of 10^{11} genomic particles of rAAV6 encoding endostatin and angiostatin rAAV-(E+A) as bicistronically expressed proteins from a single vector or rAAV encoding GFP to determine vector-related nonspecific effects. Three different time points were chosen for treatment: week 5 when the animals did not develop any abnormality in the prostate, week 10 when low to moderate PIN lesion was observed in untreated mice, and week 18 when mice showed significant adenocarcinoma characterized by well-differentiated tumor. Serum samples obtained before vector injection and regularly after therapy were subjected to ELISA for endostatin and VEGF levels. The mean serum endostatin level after rAAV-(E+A) treatment was 912 ng/mL. In untreated naïve mice, the mean endostatin level was 189 ng/mL (Fig. 1*A*). The mean serum angiostatin level after rAAV-(E+A) treatment was 651 ng/mL. In untreated naïve mice, the mean angiostatin level was 34 ng/mL (Fig. 1*B*). The systemic levels of endostatin angiostatin were comparable between rAAV-(E+A) groups after vector administration irrespective of the stage of disease and time of vector administration (Fig. 1*A* and *B*).

However, there was a marked difference in serum VEGF levels between different groups based on time of vector injection, as shown in Fig. 1*C*. In naïve mice, VEGF levels started to show significant elevation at 10 weeks of age and there was a steady increase until 32 weeks. When rAAV-(E+A) therapy was given at either 5 or at 10 weeks of age, VEGF levels showed marked decrease at 12 weeks compared with naïve mice and remained around this amount until 60 weeks ($P < 0.04$). However, in mice administered with rAAV-(E+A) at 18 weeks, when the cancer has already progressed to differentiated stage, there was no significant decrease in serum VEGF level compared with naïve animals ($P > 0.05$).

Histopathology and immunohistochemistry. To analyze the effect of sustained antiangiogenic therapy on multistage progression of prostate cancer, 22 mice from each group were sacrificed at

12, 18, 20, 24, and 32 weeks of age. Prostate tissue sections were H&E stained and graded. In rAAV-GFP–treated mice, progression of the disease was identical to that of naïve mice displaying high-grade PIN lesion by week 12, well-differentiated tumor by week 18, and poorly differentiated tumor by 24 to 28 weeks. Metastasis, especially to lung and lymph nodes, was apparent by 28 weeks in these mice as in naïve mice. However, when mice received rAAV-(E+A) treatment either at week 5 or at week 10 of age, progression of the disease was significantly slow. As shown in Fig. 2*A* and *B*, there was a significant delay in the progression of the disease. Until 18 weeks, histology of the prostate seemed normal as seen in nontransgenic littermates. However, during this time, untreated TRAMP mice exhibited high-grade PIN lesion. Around 24 weeks of age, when untreated mice already displayed poorly differentiated tumor with metastasis to liver, lung, and lymph nodes, rAAV-(E+A)–treated mice showed only well-differentiated tumor. Interestingly, prostate cancer in most of the mice in rAAV-(E+A)–treated group did not progress to poorly differentiated tumor even at 60 weeks.

Our scoring system was based on assigning the occurrence of the highest-grade tumor in the prostate irrespective of quantity of accompanying low-grade tumor cells. Hence, to discern whether differences exist in the percentage of phenotypically distinct cell populations within the same prostate tissue sample between naïve and rAAV-(E+A)–treated animals, well-differentiated prostate tumors were analyzed for percentage of cells with early-stage morphology. Results, shown in Table 1, indicated that only 10% of tissue section area was of well-differentiated type in rAAV-(E+A) treatment, whereas 90% of them were of normal to PIN lesion type. However, in naïve animals with well-differentiated tumor, none of the cells contained normal epithelial phenotype or early PIN lesion, and 40% of the scored tumors were of a well-differentiated tumor type. The occurrence of well-differentiated tumor ranged between 18 and 24 weeks in untreated animals, whereas in mice treated with rAAV-(E+A) at early stages, well-differentiated tumor was evident only after 24 weeks of age, and remained until 50 weeks (Table 1).

To determine the effects of endostatin and angiostatin from rAAV on proliferation, apoptosis, and microvessel density of the prostate, immunohistochemistry was done with anti-Ki67, anti-PARP p85 fragment, and anti–CD31/PECAM-1 antibodies, respectively. Representative results of these analyses are shown in Fig. 2*C*. There was a marked decrease in tumor cell proliferation in rAAV-(E+A)–treated mice compared with control or rAAV-GFP–treated mice. When tumor cell proliferation was compared within same grade tumors between naïve and rAAV-(E+A) groups, prominent Ki67 staining was seen in 14% of stromal cells, 62% of basal epithelial cells, and 65% of luminal epithelial cells in untreated animals. However, in the group of mice that were treated with rAAV-(E+A), the number of proliferating cells in the basal and luminal region of the prostate was 25% and 40%, respectively. There was no significant difference in the frequency of Ki67-positive stromal cells between naïve and rAAV-(E+A) groups.

Microvessel density was analyzed in the prostate tissue from 10 control and 10 rAAV-(E+A)–treated mice with the same tumor grade; there was a significant decrease in E+A–treated animals compared with the naïve group (Fig. 2*C*). The difference was more pronounced in well-differentiated and moderately differentiated tumors ($P < 0.005$), correlating to an earlier and rapid metastatic event in naïve animals. During early stages of tumor development in transgenic mice, foci of hyperplasia in the prostatic glands were observed with few newly formed vessels inside the hyperplastic lesions. With tumor progression, new blood vessel formation was seen inside the acini associated with papillary and cribiform proliferation of epithelium into the lumen. During the progression of tumor, there was an increase in the number and diameter of blood vessels both in the tumor area and in the stroma. When we measured the vessel diameter of 24-week-old naïve mice with tumors between well-differentiated to moderately differentiated grade, the diameter of blood vessels in the tumor was 17.8 ± 1.3 μm.

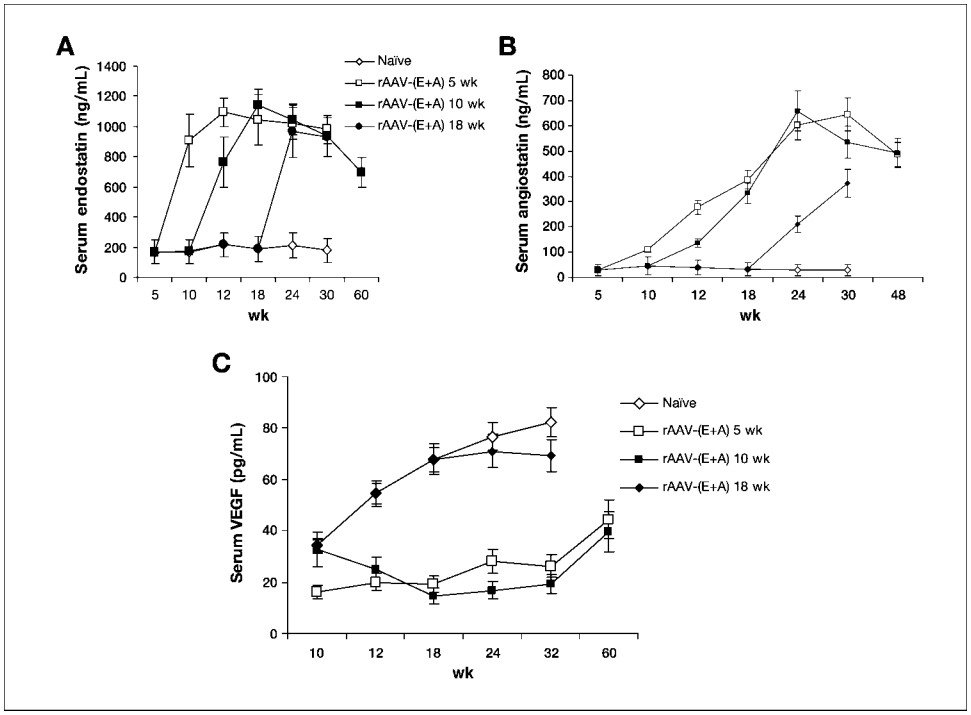

Figure 1. Serum endostatin, angiostatin, and VEGF levels. Serum samples were obtained at different time points from naïve and rAAV-(E+A)–treated mice. ELISA for human endostatin (*A*) was done using a commercial kit and that for angiostatin (*B*) by a method developed in our laboratory, described in Materials and Methods. *Points,* average of assays done in triplicate from different groups. *C,* serum VEGF levels in naïve and rAAV-(E+A)–treated mice were measured by ELISA. *Points,* average from at least 10 animals for each time point ($P < 0.003$ between ■ and ◇).

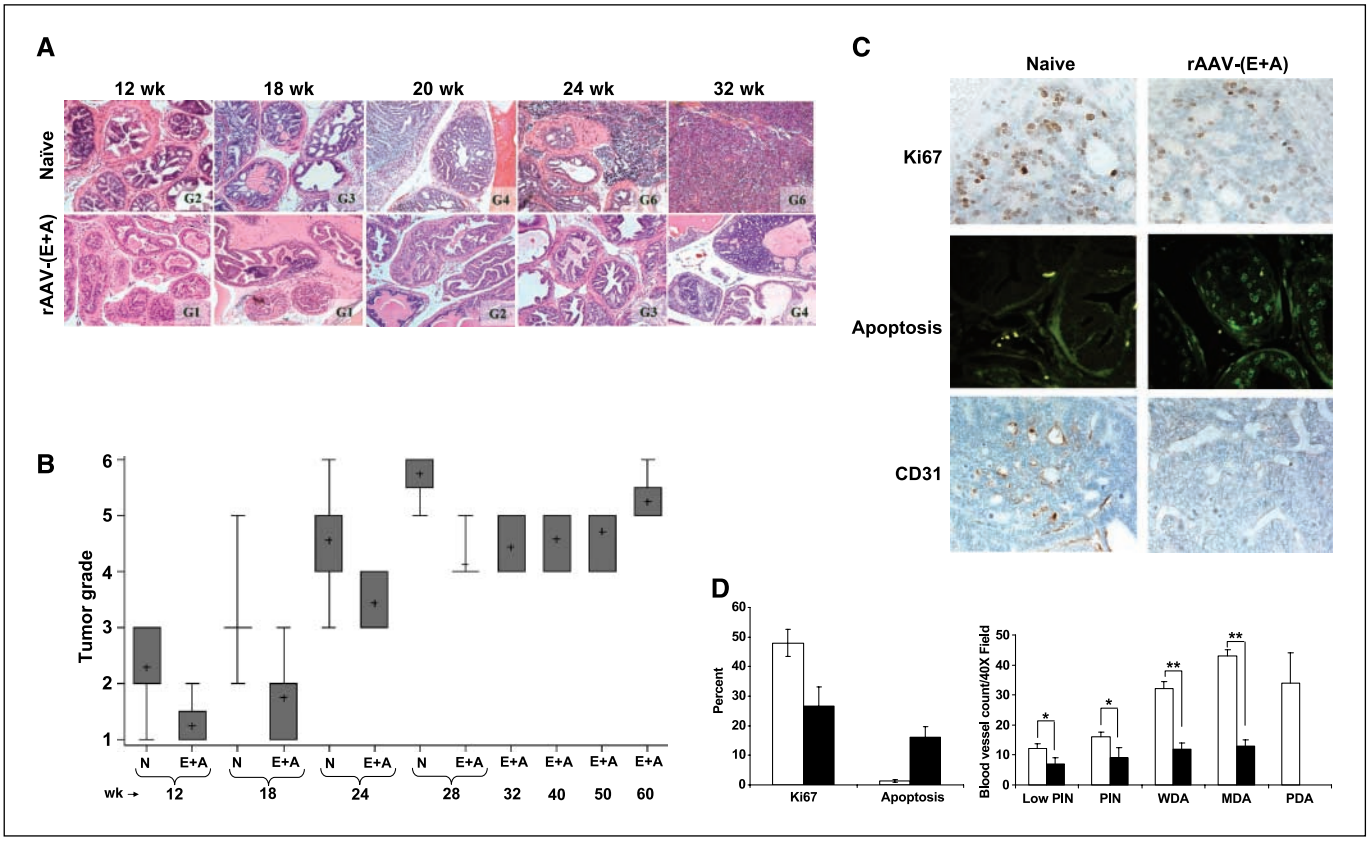

Figure 2. Histologic and immunochemical analysis of prostate tissue from TRAMP mice with or without rAAV-(E+A) treatment. *A,* cohorts of TRAMP mice were sacrificed at indicated weeks after no treatment or treatment with rAAV-(E+A), and prostate tissues were sectioned and stained for histopathology. The slides were evaluated by a pathologist and graded as follows: *G1,* grade1, normal prostate; *G2,* grade 2, low-grade PIN; *G3,* grade, high-grade PIN; *G4,* grade 4, well-differentiated tumor; *G5,* grade 5, moderately differentiated tumor; and *G6,* grade 6, poorly differentiated tumor. *B,* tumor progression in naïve and rAAV-(E+A)–treated mice over time (n = 22 mice per group). *C,* for immunochemistry analysis of tumor cell proliferation, apoptosis, and microvessel density in naïve (24 wks) and rAAV-(E+A)–treated (48 wks) TRAMP mice, prostate tissues obtained from mice with the same histologic grade (well-differentiated tumor) were paraffin embedded and sectioned. Staining was done with anti-Ki67 antibody for proliferation, anti-PARP p85 fragment polyclonal antibody for apoptosis, and CD31/PECAM-1 antibody for endothelial cells. The slides were minimally counterstained with hematoxylin. *D,* proliferation and apoptotic indices were calculated by counting positive cells in 10 random fields at ×40 magnification from naïve (*open columns*) and rAAV-(E+A)–treated (*filled columns*) mice having well-differentiated tumor ($P < 0.004$ for proliferation and $P < 0.003$ for apoptosis). Blood vessel counts were determined by counting the number of vessels in 10 randomly chosen areas of CD31/PECAM-1–stained sections in high power (*, $P < 0.02$ and **, $P < 0.005$). All of the analyses were done at least in 10 mice per group. *WDA,* well-differentiated tumor; *MDA,* moderately differentiated tumor; *PDA,* poorly differentiated tumor.

However, in mice treated with rAAV-(E+A), this grade tumor was evident only around 48 weeks of age. Interestingly, the diameter of vessels in the prostate tumor of rAAV-(E+A)–treated group was 11.5 ± 0.6 μm ($P < 0.001$). In the stromal compartment, the treated group showed a mean blood vessel diameter of 49.3 ± 12.1 μm, whereas in untreated mice the vessel diameter was found to be 124.3 ± 27.7 μm ($P < 0.0001$). Apoptotic index in the rAAV-(E+A)–treated group was eight times higher than in naïve mice and the rAAV-GFP–treated mice in all tumor grades ($P < 0.003$; Fig. 2*D*).

Long-term survival and organ metastasis. Results of long-term survival are given in Fig. 3*A*. Following rAAV-(E+A) administration at 5 and 10 weeks of age, significant increase in survival was recorded and >60% of mice were alive even after 60 weeks ($P < 0.003$). However, i.m. administration of the vector at week 18, when mice had high-grade PIN lesion to well-differentiated tumor of the prostate, did not improve survival significantly ($P > 0.05$). Mean weight of the genitourinary system, consisting of the bladder, urethra, seminal vesicles, and ampullary glands from control and rAAV-(E+A) treatment at 5 or 10 weeks of age, indicated a significant reduction after treatment both during well differentiated ($P < 0.05$) and moderately differentiated ($P = 0.001$) stages (Fig. 3*B*). The increase in survival after endostatin and angiostatin therapy also correlated with an absence of organ metastasis. Mice that were untreated or given rAAV-GFP had visible metastasis of the cancer to organs including lung, spleen, lymph nodes, and liver around 20 weeks, whereas no distant

Table 1. Percentage of prostate cancer cells based on phenotype in grade 4 tumors of naïve and rAAV-(E+A)–treated mice

	Age range (wk)	Normal (%)	Low PIN (%)	High PIN (%)	Well-differentiated tumor (%)	Total (%)
Naïve	18-24	0	0	60 ± 14	40 ± 16	100
rAAV-(E+A)	24-60	16 ± 8	7 ± 4	67 ± 25	10 ± 7	100

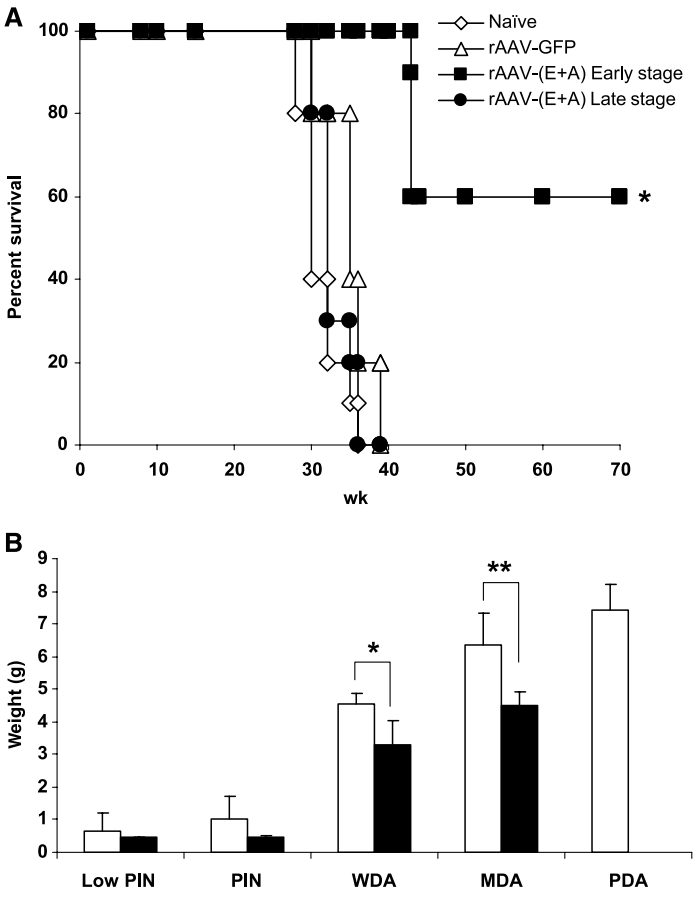

Figure 3. Survival index, urinogenital system, and metastasis in TRAMP mice after rAAV-(E+A) treatment. *A,* survival was recorded from 14 mice in each group. rAAV-(E+A) early stage indicates treatment given at 5 or 10 wks; rAAV-(E+A) late stage indicates treatment given at 18 wks. *, $P < 0.003$ compared with naïve and rAAV-GFP. *B,* mouse genitourinary tracts consisting of bladder, urethra, seminal vesicles, ampullary gland, and the prostate were excised and weighed at different stages of tumor progression from naïve (*open columns*) and rAAV-(E+A)–treated (*filled columns*) mice. The stages included PIN, well-differentiated tumor, moderately differentiated tumor, and poorly differentiated tumor. The tissues were weighed and the mean weight was determined (*, $P < 0.05$; **, $P < 0.001$). *C,* metastasis to liver, lung, and lymph nodes was analyzed by H&E staining from naïve and rAAV-(E+A)–treated mice 32 wks of age. *Arrows,* metastatic foci.

metastasis was found in rAAV-(E+A)–treated mice until 48 weeks (Fig. 3*C*).

Expression of VEGF receptors, Hif-1α, and synaptophysin. Previous studies have characterized that during early events of cancer development in TRAMP mice, expression of Hif-1α and VEGFR-1 (Flt-1) is up-regulated but as the disease progresses, expression of VEGFR-2 (KDR/Flk-1) is increased (17). Because we observed significant decrease in serum VEGF levels after rAAV-(E+A) gene therapy, given either before the onset or during early stages of the disease, we sought to determine if stable expression of these factors resulted in modulating the expression of Hif-1α and VEGF receptors. Prostate tissues obtained at different time points from naïve and rAAV-(E+A)–treated mice were immunohistochemically stained for the expression of Hif-1α, VEGFR1, and VEGFR2. To identify whether cells positive for the expression of these factors were of tumor origin or of proliferating endothelial cell origin, the same slides were also stained with antibodies for cytokeratin-8 and CD31, respectively. In untreated mice, expression of Hif-1α and VEGFR1 were predominant during early stages of tumor growth (until week 12). There was no significant difference in the expression of Hif-1α and VEGFR1 in the endothelial cells of naïve and rAAV-(E+A)–treated mice; however, there was a moderate reduction in VEGFR1 expression in tumor cells of rAAV-(E+A)–treated animals (data not shown). In contrast, staining for VEGFR2 indicated a significant decrease in expression after rAAV-(E+A) therapy given at either 5 or 10 weeks of age. In untreated mice, highly intense staining for VEGFR2 was observed from week 12 and continued throughout their life span. However, when rAAV-(E+A) therapy was given either at 5 or 10 weeks of age, VEGFR2 expression was significantly reduced (Fig. 4*A*). This difference was seen both in tumor cells and in tumor endothelium by colocalization studies. Real-time PCR analysis of RNA samples isolated from the tumor tissues also corroborated the results of immunohistochemistry (Fig. 4*B*).

To determine if antiangiogenic therapy impairs the onset of neuroendocrine transition of prostate epithelial tumors, areas of well/poorly differentiated tumors from naïve and rAAV-(E+A)–treated mice were stained with synaptophysin, a marker for neuroendocrine differentiation. Although high-level expression of synaptophysin is not observed in well-differentiated tumors in the prostate of TRAMP, compared with rAAV-(E+A)–treated animals that showed no staining, regions of well-differentiated tumor in naïve mice showed sporadic, positively stained cells adjacent to regions of poor differentiation with intense staining for synaptophysin. Quantitation of synaptophysin-positive cells in the prostate of moderately-differentiated tumor indicated 38% in untreated mice and 14% after rAAV-(E+A) treatment ($P < 0.05$; Fig. 5).

Endostatin and angiostatin treatment significantly decreases proliferation of endothelial cells and nonmetastatic prostate cancer cells. Data from *in vivo* studies corroborated with *in vitro* analysis of cell proliferation and VEGFR-2 expression. Treatment of nonmetastatic TRAMP-C3 and metastatic TRAMP-C2 and HUVEC

with endostatin and angiostatin by gene transfer indicated a significant difference in cell proliferation only in TRAMP-C3 and HUVEC (Fig. 6*A*). Interestingly, RT-PCR analysis for VEGFR-2 indicated significant down-regulation after treatment with endostatin and angiostatin in TRAMP-C2, TRAMP-3, and HUVEC (Fig. 6*B*), suggesting a possible involvement of additional proangiogenic factors that mediate aggressive growth pattern through different signal pathways, which may limit the antiangiogenic effects of endostatin and angiostatin therapy *in vivo*.

Discussion

Antiangiogenesis is a promising new therapy for prostate cancer. Although early clinical trials targeting tumor angiogenesis with purified proteins or pharmacologic drugs have shown promise, the effects have only been transient (18, 19). Most of these trials have enrolled patients having end-stage cancer with an aggressive phenotype and highly established vascular network (20–22). Although antiangiogenic therapy targets tumor vasculature rather than tumor cells directly, the onset of metastasis triggers a cascade of signaling events in cancer cells, tumor endothelium, and cells of the matrix. Thus, targeting the event of angiogenesis by specific antiangiogenic compounds for antitumor effects requires identification of an optimal stage of tumor growth for therapeutic intervention. Many of the preclinical animal studies validating antiangiogenic drugs, recombinant factors, and gene transfer approaches have been done in immunodeficient animals (23–26). Despite promising results, in these models, the kinetics of implanted tumor growth and the relevance of cell lines studied to the pattern of primary growth and spontaneous progression of human tumor are highly limited.

The present study sought to determine the effects of sustained antiangiogenic therapy, initiated at different stages of tumor progression and characterized by distinct histologic grade, in an autochthonous TRAMP model. A combination of endostatin and angiostatin was used as antiangiogenic factors by a stable gene therapy approach based on its proven efficacy in our previous studies (8, 9). Recent studies have identified cellular targets that bind angiostatin, including, $\alpha_v\beta_3$ integrin (27), ATP synthase (28), and CD26 (29). Endostatin has been reported to mediate its antiangiogenic effects by binding to integrin $\alpha_5\beta_1$ (30) and VEGFR-2 present on endothelial cells and cancer cells (31, 32), inhibition of matrix metalloproteinases (32), and down-regulation of c-*myc* and cyclin-D1 (33). On the other hand, there is a clear correlation on VEGF level and expression of VEGF receptors during the progression of prostate cancer both in human patients and in mice prone to developing spontaneous prostatic neoplasia (7, 17, 34). During the initial stages of prostate disease, characterized by PIN lesion, increased levels of VEGFR1 and Hif-1α have been reported (17). As the disease progresses to the onset of metastasis, VEGFR2 level becomes pronounced with a decrease in VEGFR1 and Hif-1α. Results of the present study indicate that despite

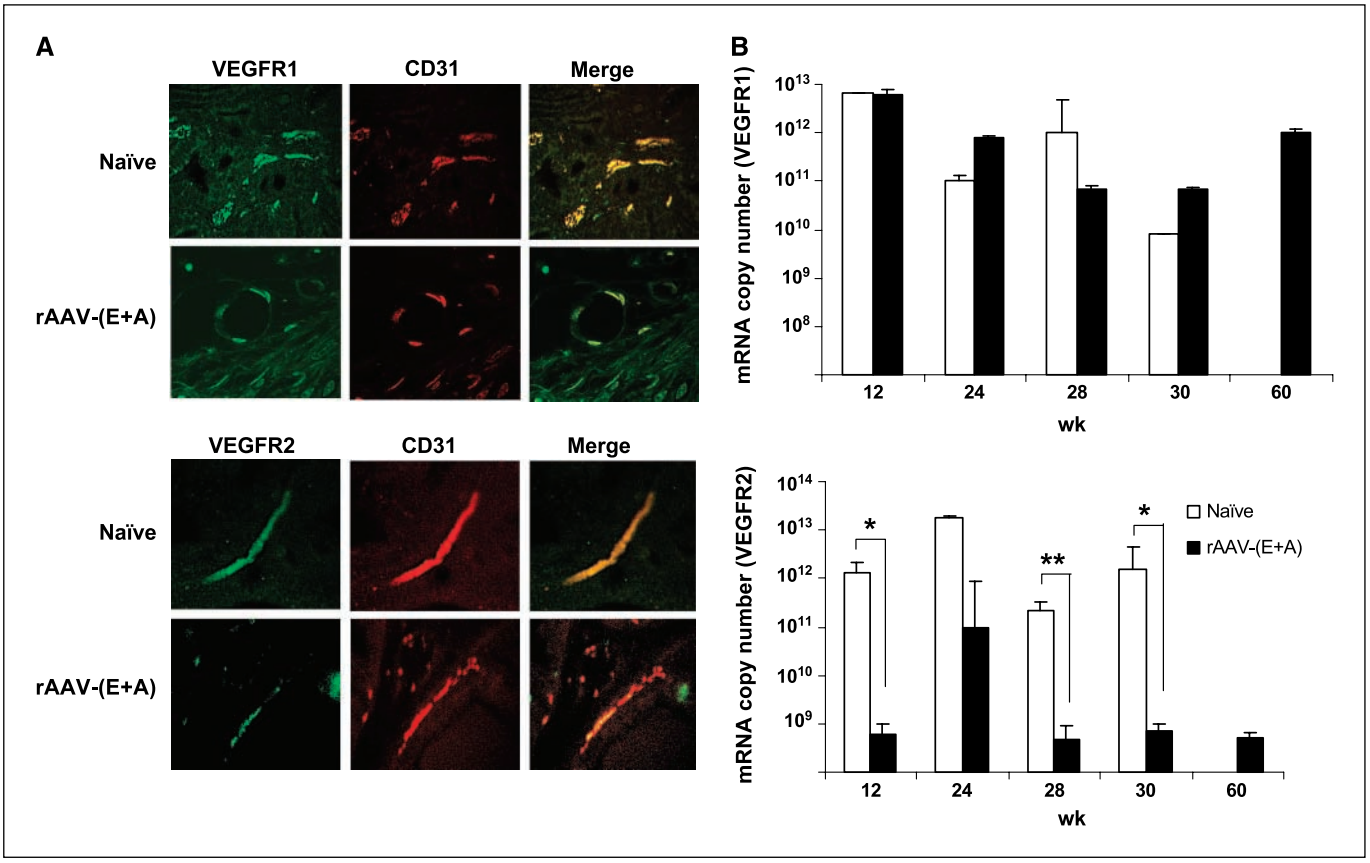

Figure 4. Expression of VEGFR1 and VEGFR2 in proliferating tumor endothelium in naïve and rAAV-(E+A)–treated mice. *A,* paraffin sections of prostate tissue from naïve and rAAV-(E+A)–treated mice with the same grade tumor were stained with antibodies for VEGFR1 (*top*) or VEGFR2 (*bottom*) and CD31. Images obtained from individual staining were also merged to show relative expression of the receptors on endothelial cells after treatment. *B,* quantitative real-time PCR analysis of VEGFR1 and VEGFR2 from RNA isolated from naïve and rAAV-(E+A)–treated TRAMP mice (treated at 5 wks of age) at different stages. *Columns,* copy number of VEGFR mRNA, normalized to copy number of GAPDH amplification from the same sample ($n = 22$ per group; *, $P < 0.025$ and **, $P < 0.05$ compared with naïve mice).

maintenance of elevated levels of antiangiogenic factors systemically, the effects were highly significant only when the therapy was initiated at early stages of cancer. Interestingly, similar antitumor effects of endostatin and angiostatin were seen whether therapy was initiated before the onset of cancer around 5 weeks or when PIN lesions already became apparent at 10 weeks. Thus, it is suggestive that antiangiogenic therapy may be more effective when started before or during early angiogenic switch of tumor progression, and before the acquisition of a more aggressive, metastatic phenotype. The same therapy when given at later stages of tumor may be ineffective because preexisting vessels may no longer be viable targets. Although, in our studies, the VEGFR-2 levels were higher during this time compared with other time points, interestingly, a similar increase in VEGFR-2 levels was also observed in untreated mice during the same time. Previous experimental therapeutic studies using TRAMP mice have also reported that the highest levels of VEGFR-2 expression occurred during this time, beginning at 16 weeks (17). Based on this observation, we speculate that systemically sustained levels of endostatin and angiostatin during VEGFR-1 and VEGFR-2 signaling axis that is sufficient to impair tumor angiogenesis and acquisition of metastatic phenotype may extend long-term survival.

VEGF signaling through VEGFR2 has been known to initiate a cascade of downstream activation involving p38 mitogen-activated protein kinase (MAPK), phosphatidylinositol 3-kinase (PI3K), and Src leading to endothelial and tumor cell proliferation and migration, leading to metastasis. Signaling through MAPK, PI3K, and Src pathways results in the up-regulation of other angiogenic factors such as platelet-derived growth factor, insulin-like growth factor, and epidermal growth factor (35–37). Hence, antiangiogenic therapy targeting VEGF would be more effective during early transitional stages of prostate cancer progression by not only impairing the metastatic switch but also indirectly affecting the activation of other factors that trigger metastatic events. Direct binding of endostatin to VEGFR2 has been shown to block VEGF-mediated signaling (32). Recent studies have also indicated that endostatin possibly exerts a sequestering effect on VEGF in tumor cells that precludes its release and subsequent recruitment of new vasculature (38).

The antiangiogenic effect of angiostatin has been attributed to its binding to $\alpha_v\beta_3$ integrin, ATP synthase, and CD26 (27–29). The integrin receptor $\alpha_v\beta_3$ has been shown to play a critical role in tumor metastasis (39). Its expression is up-regulated in newly synthesized blood vessels. Results of immunohistochemistry with CD31/PECAM antibody in the present study also concur with previous findings in TRAMP model that there is a direct correlation between increased microvessel density and progressive stages of cancer, beginning with low-grade PIN lesion. However, no increase in microvessel density was observed in prostate tissue of nontransgenic mice of the same age (7, 17, 40). Thus, the effects of angiostatin and endostatin therapy when initiated during early phases of tumor growth seem to be more significant than when given for advanced-stage disease.

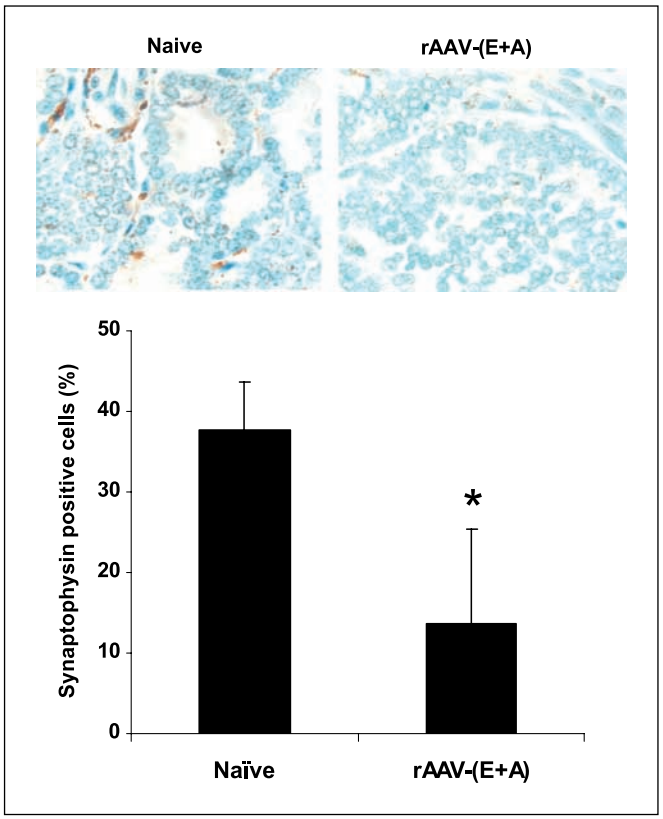

Figure 5. Synaptophysin expression in prostate tissue of naïve and rAAV-(E+A)–treated mice. Prostate from naïve and rAAV-(E+A)–treated mice having differentiated tumor were stained with synaptophysin antibody. Compared with rAAV-(E+A)–treated animals, which showed no staining, well-differentiated tumor cells of naïve mice showed sporadic, positively stained cells. *Columns,* percentage of synaptophysin-positive cells between the two groups (*, $P < 0.05$).

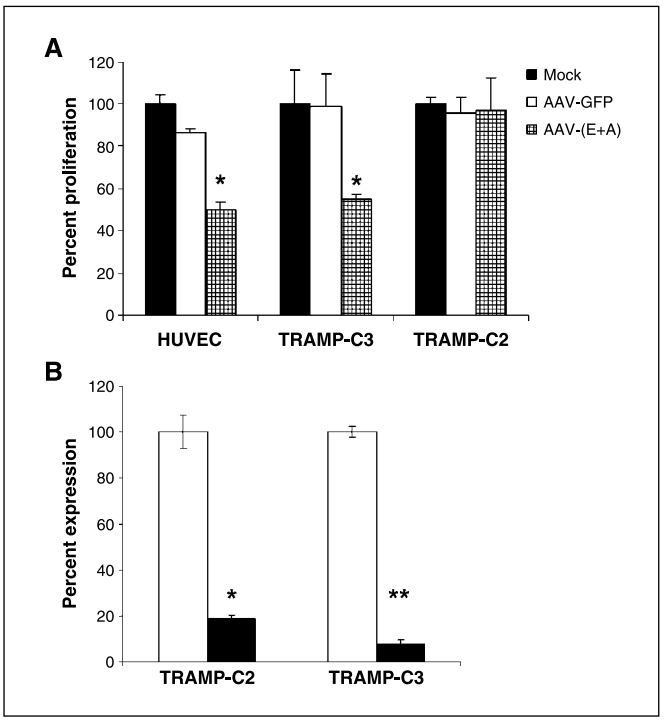

Figure 6. Effects of endostatin and angiostatin on proliferation and VEGFR expression in TRAMP-C2, TRAMP-C3, and HUVEC *in vitro*. *A,* cell proliferation was determined by 3-(4,5-dimethylthiazol-2-yl)-2,5-diphenyltetrazolium bromide assay in nontransfected or rAAV-GFP or rAAV-(E+A) cells (*, $P < 0.005$ compared with mock). *B,* RT-PCR analysis for the expression of VEGFR-2 was done with total RNA isolated from mock-transfected (*open columns*) and AAV-(E+A)–transfected (*filled columns*) TRAMP-C2 and TRAM-C3 cells 48 h after gene transfer. Relative copy number of the RNA transcripts was determined by normalizing with values obtained from amplification of GAPDH RNA (*, $P < 0.05$ and **, $P < 0.01$ compared with mock).

The acquisition of a neuroendocrine phenotype is a salient feature of late-stage prostate cancer (41). Our studies examining synaptophysin expression in differentiated areas of tumors of naïve mice indicated few synaptophysin-positive cells in well-differentiated epithelium, adjoining highly synaptophysin-positive, and poorly differentiated regions. However, there were hardly any synaptophysin-expressing cells among well-differentiated tumors of rAAV-(E+A)–treated mice prostate, suggesting that targeting angiogenesis may also delay or prevent the phenotypic switch of prostate cancer to the neuroendocrine type possibly by deprivation of oxygen and nutrients.

Further studies on the effects of antiangiogenic therapy in hormone refractory tumors characterized by neuroendocrine transition and identification of other targets modulated by angiostatin and endostatin therapy at different stages of tumor progression could provide new clues to precisely understanding the molecular interactions involved and may lead to the development of more effective targeted therapies.

Acknowledgments

Received 10/2/2006; revised 3/15/2007; accepted 4/11/2007.

Grant support: NIH grant R01CA98817 and the U.S. Army Department of Defense grants PC020372 and PC050949.

The costs of publication of this article were defrayed in part by the payment of page charges. This article must therefore be hereby marked *advertisement* in accordance with 18 U.S.C. Section 1734 solely to indicate this fact.

We thank Dr. Robert Hardy and April White for critical reading of the manuscript.

References

1. Jemal A, Siegel R, Ward E, et al. Cancer statistics, 2006. CA Cancer J Clin 2006;56:106–30.
2. Konety BR, Eastham JA, Reuter VE, et al. Feasibility of radical prostatectomy after neoadjuvant chemohormonal therapy for patients with high risk or locally advanced prostate cancer: results of a phase I/II study. J Urol 2004;171:709–13.
3. Koukourakis MI, Touloupidis S. External beam radiotherapy for prostate cancer: current position and trends. Anticancer Res 2006;26:485–94.
4. Acher PL, Morris SL, Popert RJ, Perry MJ, Potters L, Beaney RP. Permanent prostate brachytherapy: a century of technical evolution. Prostate Cancer Prostatic Dis 2006;9:215–20.
5. Masiero L, Figg WD, Kohn EC. New anti-angiogenesis agents: review of the clinical experience with carboxyamido-triazole (CAI), thalidomide, TNP-470 and interleukin-12. Angiogenesis 1997;1:23–35.
6. Figg WD, Kruger EA, Price DK, Kim S, Dahut WD. Inhibition of angiogenesis: treatment options for patients with metastatic prostate cancer. Invest New Drugs 2002;20:183–94.
7. Gingrich JR, Barrios RJ, Foster BA, Greenberg NM. Pathologic progression of autochthonous prostate cancer in the TRAMP model. Prostate Cancer Prostatic Dis 1999;2:70–5.
8. Ponnazhagan S, Mahendra G, Kumar S, et al. Adeno-associated virus 2-mediated antiangiogenic cancer gene therapy: long-term efficacy of a vector encoding angiostatin and endostatin over vectors encoding a single factor. Cancer Res 2004;64:1781–7.
9. Isayeva T, Ren C, Ponnazhagan S. Recombinant adeno-associated virus 2-mediated antiangiogenic prevention in a mouse model of intraperitoneal ovarian cancer. Clin Cancer Res 2005;11:1342–7.
10. Aldrich WA, Ren C, White AF, et al. Enhanced transduction of mouse bone marrow-derived dendritic cells by repetitive infection with self-complementary adeno-associated virus 6 combined with immunostimulatory ligands. Gene Ther 2006;13:29–39.
11. Foster BA, Gingrich JR, Kwon ED, et al. Characterization of prostatic epithelial cell lines derived from transgenic adenocarcinoma of the mouse prostate (TRAMP) model. Cancer Res 1997;57:3325–30.
12. Greenberg NM, DeMayo F, Finegold MJ, et al. Prostate cancer in a transgenic mouse. Proc Natl Acad Sci U S A 1995;92:3439–43.
13. Samulski RJ, Chang LS, Shenk TA. Recombinant plasmid from which an infectious adeno-associated virus genome can be excised *in vitro* and its use to study viral replication. J Virol 1987;61:3096–101.
14. Grimm D, Kay MA, Kleinschmidt JA. Helper virus-free, optically controllable, and two-plasmid-based production of adeno-associated virus vectors of serotypes 1 to 6. Mol Ther 2003;7:839–50.
15. Zolotukhin S, Byrne BJ, Mason E, et al. Recombinant adeno-associated virus purification using novel methods improves infectious titer and yield. Gene Ther 1999;6:973–85.
16. Suttie A, Nyska A, Haseman JK, Moser GJ, Hackett TR, Goldsworthy TL. A grading scheme for the assessment of proliferative lesions of the mouse prostate in the TRAMP model. Toxicol Pathol 2003;31:31–8.
17. Huss WJ, Hanrahan CF, Barrios RJ, Simons JW, Greenberg NM. Angiogenesis and prostate cancer: identification of a molecular progression switch. Cancer Res 2001;61:2736–43.
18. DeMoraes ED, Fogler WE, Grant D. Recombinant human angiostatin (rhA): a phase I clinical trial assessing safety, pharmacokinetics (PK) and pharmacodynamics (PD). Proc Am Soc Clin Oncol 2001;20:3a.
19. Eder JP, Supko JG, Clark JW, et al. Phase I clinical trial of recombinant human endostatin administered as a short intravenous infusion repeated daily. J Clin Oncol 2002;20:3772–84.
20. Herbst RS, Hess KR, Tran HT, et al. Phase I study of recombinant human Endostatin in patients with advanced solid tumors. J Clin Oncol 2002;20:3792–803.
21. Thomas JP, Arzoomanian RZ, Alberti D, et al. A phase I pharmacokinetic and pharmacodynamic study of recombinant human endostatin in patients with advanced solid tumors. J Clin Oncol 2003;21:223–31.
22. Kulke MH, Bergsland EK, Ryan DP, et al. Phase II study of recombinant human endostatin in patients with advanced neuroendocrine tumors. J Clin Oncol 2006;24:3555–61.
23. Muramaki M, Miyake H, Hara I, Kamidono S. Synergistic inhibition of tumor growth and metastasis by combined treatment with TNP-470 and docetaxel in a human prostate cancer PC-3 model. Int J Oncol 2005;26:623–8.
24. Nicholson B, Gulding K, Conaway M, Wedge SR, Theodorescu D. Combination antiangiogenic and androgen deprivation therapy for prostate cancer: a promising therapeutic approach. Clin Cancer Res 2004;10:8728–34.
25. Inoue K, Slaton JW, Eve BY, et al. Interleukin 8 expression regulates tumorigenicity and metastases in androgen-independent prostate cancer. Clin Cancer Res 2000;6:2104–19.
26. Raikwar SP, Temm CJ, Raikwar NS, Kao C, Molitoris BA, Gardner TA. Adenoviral vectors expressing human endostatin-angiostatin and soluble Tie2: enhanced suppression of tumor growth and antiangiogenic effects in a prostate tumor model. Mol Ther 2005;12:1091–100.
27. Tarui T, Miles LA, Takada Y. Specific interaction of angiostatin with integrin $\alpha(v)\beta(3)$ in endothelial cells. J Biol Chem 2001;276:39562–8.
28. Moser TL, Stack MS, Asplin I, et al. Angiostatin binds ATP synthase on the surface of human endothelial cells. Proc Natl Acad Sci U S A 1999;96:2811–6.
29. Gonzalez-Gronow M, Grenett HE, Gawdi G, Pizzo SV. Angiostatin directly inhibits human prostate tumor cell invasion by blocking plasminogen binding to its cellular receptor, CD26. Exp Cell Res 2005;303:22–31.
30. Sudhakar A, Sugimoto H, Yang C, Lively J, Zeisberg M, Kalluri R. Human tumstatin and human endostatin exhibit distinct antiangiogenic activities mediated by $\alpha_v\beta_3$ and $\alpha_5\beta_1$ integrins. Proc Natl Acad Sci U S A 2003;100:4766–71.
31. Hajitou A, Grignet C, Devy L, et al. The antitumoral effect of endostatin and angiostatin is associated with a down-regulation of vascular endothelial growth factor expression in tumor cells. FASEB J 2002;16:1802–4.
32. Kim YM, Hwang S, Kim YM, et al. Endostatin blocks vascular endothelial growth factor-mediated signaling via direct interaction with KDR/Flk-1. J Biol Chem 2002;277:27872–9.
33. Hanai J, Dhanabal M, Karumanchi SA, et al. Endostatin causes G1 arrest of endothelial cells through inhibition of cyclin D1. J Biol Chem 2002;277:16464–9.
34. Pallares J, Rojo F, Iriarte J, Morote J, Armadans LI, de Torres I. Study of microvessel density and the expression of the angiogenic factors VEGF, bFGF and the receptors Flt-1 and FLK-1 in benign, premalignant and malignant prostate tissues. Histol Histopathol 2006;21:857–65.
35. Qiao M, Shapiro P, Kumar R, Passaniti A. Insulin-like growth factor-1 regulates endogenous RUNX2 activity in endothelial cells through a phosphatidylinositol 3-kinase/ERK-dependent and Akt-independent signaling pathway. J Biol Chem 2004;279:42709–18.
36. Rak J, Yu JL, Klement G, Kerbel RS. Oncogenes and angiogenesis: signaling three-dimensional tumor growth. J Investig Dermatol Symp Proc 2000;5:24–33.
37. Weis S, Cui J, Barnes L, Cheresh D. Endothelial barrier disruption by VEGF-mediated Src activity potentiates tumor cell extravasation and metastasis. J Cell Biol 2004;167:223–9.
38. Macpherson GR, Ng SS, Forbes SL, et al. Anti-angiogenic activity of human endostatin is HIF-1-independent *in vitro* and sensitive to timing of treatment in a human saphenous vein assay. Mol Cancer Ther 2003;2:845–54.
39. Pecheur I, Peyruchaud O, Serre CM, et al. Integrin $\alpha(v)\beta3$ expression confers on tumor cells a greater propensity to metastasize to bone. FASEB J 2002;16:1266–8.
40. Kaplan-Lefko PJ, Chen TM, Ittmann MM, et al. Pathobiology of autochthonous prostate cancer in a pre-clinical transgenic mouse model. Prostate 2003;55:219–37.
41. Shah RB, Mehra R, Chinnaiyan AM, et al. Androgen-independent prostate cancer is a heterogeneous group of diseases: lessons from a rapid autopsy program. Cancer Res 2004;64:9209–16.